This is a “preproof” accepted article for Mineralogical Magazine.
This version may be subject to change during the production process.
10.1180/mgm.2025.28

How can Li be incorporated into the structure of Al-rich tourmaline?

Peter Bačík[1,2,*] and Andreas Ertl[3,4]

[1]Comenius University in Bratislava, Faculty of Natural Sciences, Department of Mineralogy, Petrology and Economic Geology, Ilkovičova 6, 842 15, Bratislava, Slovak Republic

[2]Earth Science Institute, Slovak Academy of Sciences, Dúbravská cesta 9, SK-845 28 Bratislava, Slovakia

[3]Mineralogisch-Petrographische Abt., Naturhistorisches Museum, Burgring 7, 1010 Wien, Austria

[4]Institut für Mineralogie und Kristallographie, Universität Wien, Josef-Holaubek-Platz 2, 1090 Wien, Austria

*Author for correspondence: Peter Bačík, Email: peter.bacik@uniba.sk

Abstract

Aluminium-rich tourmaline can contain significant amounts of Li. Until now, syntheses have not been successful in producing Li-rich tourmalines. Because it is still not clear how Li enters the *Y* site in tourmaline, possible short-range orders, including Li, are discussed using bond valence calculations. Structural arrangement graphs of the *Y*-site neighbourhood in the structure of elbaitic tourmalines were investigated to determine more information about their stability. Possible short-range ordering including Al and Li at the *Y* sites, with Na, Ca or □ (vacancy) at the *X* site, with Si (and Al or B) at the *T* sites and either (OH) or F at the *W* site were investigated. Tourmaline with varying amounts of Na but no Ca can only contain ≤1 *apfu* (atoms per formula unit) ^{Y}Li. This is consistent with the composition of synthetic tourmaline. Tourmaline with higher Li content (Li >1 *apfu*) can form when Ca is

https://doi.org/10.1180/mgm.2025.28 Published online by Cambridge University Press

included. Such tourmaline requires fluorine because more Li results in O1 underbonding, whereas more Al at the *Y* site leads to O1 overbonding. Underbonding of O1 is preferable for F because OH at the O1 site usually has a bond valence sum (BVS) higher than 1.00 vu (valence units) due to hydrogen bonding of H to ring oxygen atoms. Therefore, liddicoatitic tourmaline is enriched in F and is usually F-dominant. If no fluorine is available in the starting material of a tourmaline synthesis, it is likely that significant proportions of cations such as B and Al will be incorporated into the tetrahedral site. Ultimately, however, only a smaller proportion of Li can be incorporated. Tourmalines with such tetrahedral cations, which also contain a significant Ca content, could theoretically also have significant *Y*-site vacancies. In order to synthesize Li-rich tourmalines, we would therefore recommend that the starting material also contains both Ca and F.

Keywords: lithium-rich tourmaline; aluminium-rich tourmaline; crystal structure; bond valence calculations; short-range orders; tourmaline synthesis

https://doi.org/10.1180/mgm.2025.28 Published online by Cambridge University Press

Introduction

The general tourmaline formula is $XY_3Z_6(BO_3)_3[T_6O_{18}]V_3W$, where the *X* site in Al-rich and Li-bearing tourmalines is usually occupied by Na, Ca or is vacant (□) (Henry *et al.*, 2011). The *Y* site is in such tourmalines usually occupied by Al and Li, and the *Z* site is only occupied by Al. The *T* site can be occupied by Si and by minor amounts of B and Al. The *V* site is usually occupied by OH, and the *W* site by OH, O or F. The investigated samples exhibit unit-cell parameters with a = 15.6509-15.9569 Å, c = 7.0406-7.1380 Å (Burns et al., 1994; Bosi et al., 2005; Cempírek et al., 2024).

Until now, syntheses have not been successful in producing Li-rich tourmalines with >0.5 atoms per formula unit (*apfu*) ^{Y}Li. It is still not clear how Li enters the *Y* site in tourmalines. It therefore makes sense to take a closer look at which short-range ordering schemes can accommodate Li.

Natural and synthetic samples were used to investigate which Li-containing short-range ordering schemes can occur in Li-bearing Al-rich tourmalines.

Short-range ordering

Synthetic Al-rich and Li-bearing tourmalines without F, but with $^{[4]}$B and $^{[4]}$Al, are of special interest because they contain no Ca, only Na and vacancies at the *X* site and mainly Al and Li at the *Y* site (Ertl *et al.*, 2012a). Because these tourmalines (synthesized by David London) do not have such a complex composition, relationships are easier to recognize. In Table 1, all short-range orders for components that can contribute to these synthetic (denoted as) samples (the *Z* site is always occupied by Al) are listed.

Component **2.3** is related to the rossmanite end member. It is also related to the alumino-oxy-rossmanite end member (Ertl *et al.*, 2022), whereas **2.2** is related to the B-analogue of this tourmaline. It seems confirmed that the short-range order **1.3** is an essential component. Without it, it is not possible to explain the crystal-chemical formulae of these synthetic

https://doi.org/10.1180/mgm.2025.28 Published online by Cambridge University Press

tourmaline samples. The combination of these components with different short-range ordering arrangements makes it clear that the Li content in such a tourmaline containing only Na and vacancies at the *X* site will be in the range of 0–1 *apfu* Li. When correlating the components of the different short-range orders in the examined tourmalines, which were synthesized at different temperatures, it can be recognized that, with decreasing temperature, the component **2.1** increases, whereas it decreases with increasing temperature. This explains why the content of the tetrahedrally coordinated B significantly increases towards lower temperatures. There is no evidence that in these synthetic tourmalines, a short-range order occurs, where the *X* and *Y* sites are occupied as in **1.1**, but exclusively Si occupies the *T* site, and only O occupies the O1 (*W*) site. Such a short-range order may not be favourable or even unstable at such pressure/temperature conditions.

A natural Al-rich and Li-bearing tourmaline sample with a vacancy-dominant *X* site (rossmanite; Selway *et al.*, 1998) with the updated crystal chemical formula $^{X}(\square_{0.6}Na_{0.4})$ $^{Y}(Al_{2.2}Li_{0.7}\square_{0.1})$ $^{Z}Al_6$ $(BO_3)_3$ $[Si_{5.6}B_{0.4}O_{18}]$ $^{V}(OH)_3$ $^{W}[(OH)_{0.6}O_{0.3}F_{0.1}]$ (based on data in that publication with added tetrahedral B) seems to consist of the same short-range ordering schemes. A minor component may occur additionally: a short-range order with ^{X}Na, $^{Y}(Al_2\square)$, ^{T}Si and ^{W}(OH) (see also Ertl, 2023). However, the dominant component seems to be short-range order **2.1** (Table 1). This component is practically identical to the end-member formula of rossmanite.

However, natural Al- and Li-rich tourmalines with Li >1.0 *apfu* occur often. Such tourmalines contain additionally some Ca and significant amounts of F (*e.g.*, Ertl *et al.*, 2006, 2010). Many short-range ordering schemes occurring in such samples are already listed in Table 1, but additional components might also occur.

Components **3.1** and **3.2** have (Li_2Al) at the *Y* site. The combination of these components, together with short-range orders **1.1**, **1.2**, **1.4**, **1.5**, **2.1** and **2.4**, produces Li

https://doi.org/10.1180/mgm.2025.28 Published online by Cambridge University Press

contents in the range 1-2 *apfu* Li. However, component **2.4** does not appear to occur, as a summary of approximately 9000 tourmaline analyses from different lithological environments shows that for tourmaline with an average *X*-site charge of <+0.5, the maximum F amounts are <0.2 *apfu* (Henry and Dutrow, 2011). These chemical data of natural tourmalines indicate crystallographic influences. Natural tourmaline with relatively high Li contents always contains relatively high F contents. It seems that the contents of Li and F are positively correlated (see also Ertl, 2021). In order to find out whether short-range ordering schemes with Li and F (**1.4**, **1.5**, **3.1**; Table 1) are more favourable in terms of crystal chemistry than orders with Li and OH (**1.1**, **1.2**, **2.1**, **3.2**; Table 1), bond valence calculations were carried out.

Bond-valence topological modelling

The stability and structural effects of proposed short-range ordering (or components) can be determined by applying bond-valence topological modelling, which combines Bond Valence Theory and structural topology (Bačík 2025a, 2025b).

Bond-length calculations, as a part of Bond Valence Theory, are based on the following equation:

$$d_{ij} = R_0 - b \ln v_{ij}, \text{ [eq. 1]}$$

where d_{ij} is the bond length (in Å) between the two given ions, v_{ij} is the bond valence of the given bond (in *vu* – valence units), R_0 is the length of a bond for which $v_{ij} = 1$ *vu*, and b is the universal parameter for each bond (Brown, 2006).

The bond-valence topological modelling is based on bond-valence topological graphs, which represent the specific structural fragment with attached values of bond valences or lengths (Bačík, 2025a). Therefore, the first step in bond-valence topological modelling involves defining a structural fragment. Here, the selected fragment is identical to one formula unit extended to include all ZO_6 octahedra connected to the TO_4 tetrahedra of tourmaline (Fig.

https://doi.org/10.1180/mgm.2025.28 Published online by Cambridge University Press

1). The graph is then constructed, with all sites serving as vertices and bonds between them as edges of the graph (Fig. 2). The values are attached to each edge of the graph. These can be derived from the ideal bond valences calculated for each bond at each site (Bačík and Fridrichová, 2021). However, these almost always differ from empirical values due to polyhedron distortion (Ertl *et al*., 2002). Therefore, the starting model was derived from the structural model of dravite from Forshammar, which was based on the empirical data (Bačík, 2025a). From this, the bond-valence topological models of all natural and synthetic components specified in Table 1 were calculated. Moreover, ^{Y}(Al-Mn-Li) and ^{Y}(Al-Fe-Li) components, which are considered stable (Ertl and Bačík, 2020), were calculated as the reference standard (numbered **0.1** and **0.2**). In addition, the components that are alternatives to those proposed (**1.3a**, **1.3b**, **1.7**, **1.8** – Table 1) and can be considered stable (Hawthorne 1996, 2002; Bosi 2010, 2011, 2013, 2018) were also calculated, as well as the $^{Y}Li_3$ components (**1.9**, **1.10** – Table 1), that cannot be assigned to a stable end member and have never been observed in natural or synthetic tourmalines. These additional components are not charge-balanced at the specified sites because their purpose is simply to test the valence requirements of the local bonds. However, charge balancing can be achieved at other sites not listed in Table 1 (*V*, *Z*).

The process of model calculation is described by Bačík (2025a, 2025b) and Bačík and Fridrichová (2021). The calculations were relatively conservative, with minimal consideration of distortion effects to better compare components and highlight bond-valence requirements. In addition, the calculated values should be treated with caution; the difference between them serves to indicate the structural effects.

A theoretical bond-topological model for each arrangement was calculated and refined to fit the structural data from natural samples. To calibrate the modelling process, the sets with the compositions of the schorl-elbaite (Burns et al. 1994; Bosi et al. 2005a, 2005b, 2012,

https://doi.org/10.1180/mgm.2025.28 Published online by Cambridge University Press

2013, 2015; Ertl et al. 2006, 2008, 2012b, 2012c; Vereshchagin et al. 2013) , elbaite-liddicoatite (Lussier *et al*., 2011) and rossmanite-ertlite (Selway *et al*., 1998; Ertl *et al*., 2005, 2022; Kasatkin *et al*., 2024; Cempírek *et al*., 2024) solid solution series were used. The modelling results are divided into hydroxyl- (Table 2: bond valences; Table 4: bond lengths), fluor- (Table 2: bond valences; Table 5: bond lengths) and oxy-dominant (Table 3 – bond valences, Table 6 – bond lengths) components according to the occupancy of the O1 site. Bond valences and bond lengths of each component are compared with the ^{Y}(Al-Mn-Li) component. Differences larger than 0.01 *vu* and 0.01 Å are highlighted. Since the occupancy of the *Z* (completely occupied by Al) and *B* (completely occupied by B) sites has not changed, these are not listed in the bond valence tables for reasons of clarity.

Bond valence constraints

First, the ^{X}Na-bearing components were calculated to identify possible bond-valence requirements for sites adjacent to the *Y*, i.e., *X* and O1 (*W*) sites. From the bond-valence perspective, both AlMn^{2+}Li and AlFe^{2+}Li components are perfectly reasonable and can be stable with ^{X}Na and both ^{W}F and ^{W}OH occupancy. At first glance, Al_2Li and Al_3 may also be stable, but increased bond-valence sum (BVS) of the O1 and O2 anions should be balanced by ^{W}O as in darrellhenryite (or ^{V}O as in olenite), by vacancies at the *X* site, as in rossmanite, or by both, as in alumino-oxy-rossmanite.

The bond-valence effects were studied in more detail, mainly at the O1 and O2 sites. In general, more Al at the *Y* site leads to overbonding of O1, whereas more Li leads to underbonding of O1. This may influence the preference for O1 occupancy. Underbonding of O1 is preferable for F because OH at the O1 site usually has BVS higher than 1.00 *vu* (usually around 1.05 vu) due to hydrogen bonding of H to ring oxygen atoms (Hawthorne, 1996, 2002; Gatta *et al*., 2014). Overbonding of O1 leads to a higher BVS of ^{Y}Al in OH-containing liddicoatitic components (**3.2**, Table 2) compared to F-containing ones (**3.1**, Table 3).

https://doi.org/10.1180/mgm.2025.28 Published online by Cambridge University Press

Consequently, liddicoatitic tourmaline is enriched in F and is usually F-dominant (Ertl *et al.*, 2006; Lussier *et al.*, 2011). In fact, ^{W}OH dominant liddicoatite is a non-approved species, and the originally described liddicoatite has been redefined as fluor-liddicoatite (Henry *et al.*, 2011).

In the case of $^{Y}Al_3$ components **1.3a** and **1.3b**, the BVS at O1 increases to 1.59 *vu* (+0.53 *vu* compared to **0.1**) and 1.53 *vu* (+0.53 *vu* compared to **0.3**), respectively. This is a clear indication that $^{Y}Al_3$ occupancy requires the presence of ^{W}O; therefore, the **1.3** component is stable (Table 6).

Similar effects can be observed at the O2 site; it is also strongly influenced by the Al/Li ratio. This in turn sets the bond valence requirements for occupying the *X* site, which shares O2 with the *Y* site. The Al-dominant components show an increase in the BVS of O2, 2.02 *vu* for $^{Y}(Al_2Li)$ and even 2.31 *vu* for $^{Y}Al_3$ components. This can be solved in two different ways. In the $^{Y}(Al_2Li)$ component, the difference is small and within the value of Na-O2 bond valence. Consequently, the rossmanite substitution with introducing the *X*-site vacancy is the natural way to reduce the BVS at O2 and relax the possible structural strain. When $^{Y}Al_3$ components are considered, the difference is too large, but can be indirectly relaxed by replacing OH with O at O1, which changes the distribution of bond valences in *Y*-O bonds and reduces the BVS of O2 (Table 6).

In contrast, the $^{Y}(Li_2Al)$ components **1.7** and **1.8** exhibit a deficit of -0.12 *vu* in the BVS of the O2 site (Tables 4 and 5). Consequently, it is necessary to increase the BVS at O2, which can be achieved by replacing Na with Ca at the *X* site. This results in the stable components **3.1** and **3.2**, whereby the F-bearing component **3.1**, as discussed above, is significantly more common.

The components with the *Y*-site vacancy, including **1.6**, **3.3** and **3.4** (described by Ertl, 2023), are very specific because the absence of a *Y*-site cation limits the possible occupancy

https://doi.org/10.1180/mgm.2025.28 Published online by Cambridge University Press

of the other two sites in the triplet of linked YO_6 octahedra. For components to be as stable as possible, less highly charged cations are required, similar to micas, where micas with three divalent cations at octahedral sites transform into those with two trivalent octahedral cations and a vacancy (Rieder *et al*., 1998). Similarly, all proposed *Y*-site vacant components have a $^{Y}(Al_2\square)$ occupancy. The first component tested, **1.6**, does not show any significant irregularities that could unambiguously deny its existence. However, the smaller BVS at O2 suggests that the *X*-site would prefer a cation with a higher charge than Na, which would additionally contribute to the BVS of O2. Apparently, the **3.3** and **3.4** components with ^{X}Ca show reasonable BVS values for all sites, including O2. Although their values increase slightly compared to **0.1**, they correspond almost perfectly to the ideal BVS of 2 *vu* (Table 4). A good candidate for significant proportions of **3.3** and/or **3.4** is an Al-rich tourmaline from Koralpe, Austria, which has the formula $^{X}(Na_{0.40}Ca_{0.29}\square_{0.31})$ $^{Y}(Al_{2.40}Li_{0.35}\square_{0.25})$ $^{Z}Al_6$ $(BO_3)_3$ $^{T}[Si_{4.89}B_{0.83}Al_{0.27}Be_{0.01}]O_{18}$ $^{V}(OH)_3$ $^{W}[O_{0.58}(OH)_{0.36}F_{0.06}]$ (Ertl *et al*., 2007, and references therein). This tourmaline, originally described as B-rich olenite, is a complex solid solution of various end members, consisting primarily of ertlite (36 mol%) and alumino-oxy-rossmanite (16 mol%), if valid tourmaline end members and also the *V*- and *W*-site occupations are taken into account.

In contrast, the decrease in BVS at O2 in the Li_3 components is too large for a divalent substituent at the *X*-site and would require a trivalent cation at *X*. However, this is highly unlikely in natural compositions; only trivalent lanthanides from La^{3+} to Gd^{3+} with bond lengths similar to Ca^{2+} could occupy the *X* site (Bačík and Fridrichová, 2021), but their content in tourmalines is usually very limited, up to 1200 ppm in natural samples (Hellingwerf et al., 1994; Ertl et al., 2006; Novák et al., 2011; Bačík et al., 2012). Furthermore, the BVS at O1 as low as 0.53 *vu* is obviously unsuitable for any anion at this

https://doi.org/10.1180/mgm.2025.28 Published online by Cambridge University Press

site and is extremely unlikely to be relaxed by any distortion of the YO_6 octahedra. Consequently, it is almost certainly impossible to obtain a stable tourmaline with $^{Y}Li_3$.

Bond lengths of theoretical components

Equation 1 allows calculation of bond lengths from topological bond-valence models of each component using the R_0 and b values for cation-oxygen bonds from the list of Gagné and Hawthorne (2015) and for cation-fluorine bonds from Brown (2013). These are listed in Tables 5-7 in comparison to the starting components **0.1** and **0.3**. In addition, the calculated bond lengths of each component can be compared with the empirical values of the schorl-elbaite (Burns et al. 1994; Bosi et al. 2005a, 2005b, 2012, 2013, 2015; Ertl et al. 2006, 2008, 2012b, 2012c; Vereshchagin et al. 2013), the elbaite-liddicoatite (Lussier *et al*., 2011) and the rossmanite-ertlite (Selway *et al*., 1998; Ertl *et al*., 2005, 2022; Kasatkin *et al*., 2024; Cempírek *et al*., 2024) series (Fig. 3). Due to some similarities (i.e., high ^{Y}Al content and the presence of tetrahedral trivalent cations in samples examined), ertlite was added to rossmanite, even though it is an alkali tourmaline and not a tourmaline with a vacant *X* site. Comparison with natural samples makes it possible to identify functional models and distinguish them from improbable models.

All bond lengths in the YO_6 octahedron show significant negative correlations with the total Al content (Fig. 3). This is expected because ^{Y}Al content correlates with total Al and Al produces the shortest bonds among typical octahedral cations (Bačík and Fridrichová, 2021). The calculated components follow this trend and border the area in which the real samples are located.

The *Y*-O1 bond lengths clearly separate the ^{W}F-containing components with shorter bonds from the ^{W}OH-containing tourmalines. Although the *Y*-O1 bond valence is slightly weaker for O1 occupied by F, because hydrogen bonding increases the BVS of O1 with OH (Hawthorne, 1996, 2002), F generally forms shorter bonds than O for the same bond valence.

https://doi.org/10.1180/mgm.2025.28 Published online by Cambridge University Press

The ideal Al-O bond length in the octahedral coordination is 1.904 Å (Bačík and Fridrichová, 2021; calculated from Gagné and Hawthorne, 2015), whereas for the Al-O bond it is 1.801 (calculated from Brown, 2013). As expected, the natural samples followed the trend between ^{W}OH- and ^{W}F-containing components (Fig. 3a).

Comparing the total Al bond length with the *Y*-O2 bond length shows slightly different behaviour (Fig. 3b). There is no clear distinction between ^{W}OH- and ^{W}F-bearing components; most of them overlap and form a clear negative correlation trend. However, when Al > 8 *apfu*, the relatively narrow trend breaks with a larger spread between the theoretical components. Components **1.3a** and **1.3b** have an extremely shortened *Y*-O2 bond. Decreasing each *Y*-O2 bond by ca. 0.25 *vu* would result in strong underbonding of the *Y* site, making its occurrence unlikely. However, the decrease can be achieved by increasing the valence of other bonds, e.g., *Y*-O3. Consequently, components with ^{W}O, i.e., **1.3**, **2.2** and **2.3**, have a more reasonable BVS of the *Y* and O2 sites.

When comparing *Y*-O3 with total Al, most of the ^{W}OH- and ^{W}F-containing components overlap as in the previous case (Fig. 3c). However, the components with a vacant *Y* site (**1.6** and **3.4**, except **3.3**, which is on the main trend line with reasonable *Y*-O3 bond length) separated from the trend with an extremely shortened *Y*-O3 bond due to the absence of Li, which increases the average *Y*-O3 bond length in other components with total Al = 8 *apfu*. A similar extreme shortening of the average bond length is observed in the components with a vacant *Y*-site for the *Y*-O6 bond (Fig. 3d). This is also due to the absence of Li in these components. The oxy-component **2.3** is the extension of the main trend for *Y*-O3, while the other two oxy-components have shorter *Y*-O3 distances (Fig. 3c).

The distribution of *Y*-O6 bond lengths in the components is similar to *Y*-O2, with a relatively narrow trend at Al < 8 *apfu* and its scatter at Al > 8 *apfu* (Fig. 3d). The components with a vacant *Y* site have an extremely shortened *Y*-O6 bond due to the absence of Li,

https://doi.org/10.1180/mgm.2025.28 Published online by Cambridge University Press

similarly to *Y*-O3. The oxy-components with vacant *X* sites **2.2** and **2.3** have a similar *Y*-O6 bond length regardless of the total Al content, while it is shortened in **1.3** (Fig. 3d).

The metrics of the YO_6 octahedron can also be described by the sum of opposite bond lengths as O1-*Y*-O3 and O2-*Y*-O6 (twice in the octahedron) (Bačík, 2018). The *Y*-O1+*Y*-O3 and *Y*-O2+*Y*-O6 distances, calculated for theoretical components, show a similar negative correlation. The natural samples followed the trend between ^{W}OH- and ^{W}F-containing components, clearly visible in the comparison *Y*-O1+*Y*-O3 vs. total Al (Fig. 3e); theoretical components form the range in which natural samples occur. In the case of *Y*-O2+*Y*-O6 vs. total Al, ^{W}OH- and ^{W}F-containing components overlap (Fig. 3f). The natural samples follow the trend in the range limited by theoretical components even better than in the case of individual *Y*-O2 (Fig. 3b) and *Y*-O6 (Fig. 3d) bond lengths. This suggests that the valences of these bonds can balance each other and thus influence the overall distortion of the YO_6 octahedron.

Bond lengths in natural samples

The plots of bond lengths versus total Al show interesting differences between the series of natural tourmalines studied. Tourmalines of the schorl-elbaite series show a very good correlation for all bond lengths. Consequently, it can be assumed that their behaviour can be well described by the shrinkage of the YO_6 octahedra due to the increase in Al content. However, small differences in the two other series indicate the influence of the neighbouring sites.

In tourmalines of the elbaite-liddicoatite series (Lussier *et al.*, 2011), the negative correlation to total Al for *Y*-O1 is less pronounced (Fig. 3a), and the *Y*-O1 bond is shorter than in other tourmalines with similar Al content. The much flatter slope of the trend indicates a strong influence of $^{W}F^{W}(OH)_{-1}$ substitution. Antagonistic behaviour is evident in the *Y*-O2 and *Y*-O6 bond lengths; *Y*-O2 is longer in elbaite-liddicoatite than in schorl-elbaite samples,

https://doi.org/10.1180/mgm.2025.28 Published online by Cambridge University Press

whereas *Y*-O6 is shorter. This may be due to the substitution of divalent Ca by monovalent Na at the *X* site. The stronger Ca-O2 bonds cause a weakening and lengthening of *Y*-O2 bonds. This is compensated by the shortening of the opposite *Y*-O6 bonds and is accompanied by a decrease in the bond valence of *Z*-O6 to maintain the BVS of O6. The *Y*-O3 bond is longer in elbaite-liddicoatite samples, which probably compensates the increase in *Z*-O3 bond valence resulting from the bond valence from the above-mentioned decrease in the *Z*-O6 bond valence. This intricate relationship between O3 and O6 bonds has also been described in the schorl-dravite series (Bačík, 2018).

Rossmanite and ertlite samples have the highest total Al content, which in part also occupies the *T* site. Consequently, they are expected to extend the schorl-elbaite trend to higher total Al content. This can be observed for *Y*-O1 and *Y*-O3 bonds. However, the behaviour of *Y*-O2 and *Y*-O6 bonds is more complex. Rossmanite and ertlite have relatively invariant *Y*-O2 bond lengths of ca. 1.95 Å, apparently independent of total Al content. This suggests an upper limit for the *Y*-O2 bond valence of about 0.45 *vu*. This is close to the value of the *Y*-O2 bond valence used for the components **1.3** (0.44 *vu*), **2.2** and **2.3** (both 0.49 *vu*). This resulted in a slight underbonding of the *Y* site (2.92-2.97 *vu*). A similar effect can be observed for the *Y*-O6 bond, where rossmanite samples follow the vertical trend of the theoretical oxy-components **2.2**, **2.3** and **2.4**. However, this does not work for ertlite with the extremely shortened *Y*-O6, which is closer to the oxy-component **1.3**. This component also corresponds very well to the chemical composition of natural ertlite. Rossmanite (Selway *et al*., 1998; Ertl *et al*., 2005), fluor-rossmanite (Kasatkin *et al*., 2024), and alumino-oxy-rossmanite (Ertl *et al*. 2022) are *X*-site vacant and Al-rich. However, the total content of trivalent tetrahedral cations is below 1.00 *apfu*. Therefore, the increase in total Al is crystal-chemically controlled by the components **2.3** and **2.4**. The further increase in trivalent

https://doi.org/10.1180/mgm.2025.28 Published online by Cambridge University Press

tetrahedral cations over 1.00 *apfu* (up to 2 *apfu*) in ertlite (Cempírek *et al*., 2025) is enabled by the ^{X}Na-containing oxy-component **1.3**.

The last interesting question about *X*-site vacant tourmalines is whether there is a preference for *W*-site occupancy, such as in liddicoatite samples. All *X*-site vacant components (**2.1**, **2.2, 2.3** and **2.4**) seem relatively reasonable from a bond valence perspective, although the first pair has a slightly lower BVS of O2. However, when comparing the natural samples with the theoretical ones, the OH-containing component **2.1** deviates with a significantly longer *Y*-O1 bond. Natural samples are much closer to F-containing component **2.4**. This would suggest that $^{Y}(Al_2Li)$ components prefer ^{W}F. However, fluor-rossmanite has been described as a valid mineral species but only with 0.44 *apfu* F (Kasatkin *et al*., 2024). Rossmanite from the type locality Rožná, Czech Republic, has an even lower F content of 0.1 *apfu* (Selway *et al*., 1998). A closer look at the composition of all rossmanite samples reveals interesting common features – a relatively significant content of $^{W}O^{2-}$ and trivalent cations at the *T* site. This suggests that components **2.2** and **2.3** significantly influence natural samples. The resulting bond lengths are the weighted average of various components (the *X*-site vacant and others), mostly highlighted in the *Y*-O1 bond length. Although the overall composition of rossmanite from the type locality is OH-dominant, the component **2.1**, which corresponds to the end-member composition of rossmanite, may not necessarily be dominant in the crystal structure. It is a similar situation as for tourmaline from Forshammar, Sweden, which is classified as dravite (Bačík *et al*., 2012). However, the topological mapping of the bond valence revealed that component corresponding to the dravite end member is present only at 24%, and the oxy-dravite component is the most abundant (Bačík, 2025a). However, it turned out that component 2.1 most likely exists (Tables 4, 10). Therefore, rossmanite can still be classified as a common component in Li-containing tourmalines.

https://doi.org/10.1180/mgm.2025.28 Published online by Cambridge University Press

Conclusions

Based on the topological modelling of the bond valence of Al- and Li-rich tourmalines, the bond-valence constraints enabled the assessment of the probability and stability of the studied components. These can be divided into three groups: 1) Likely – components with BVS of all sites that are very close to the ideal formal valence (IFV), with a difference of less than 0.1 *vu*; 2) Reasonable – components with BVS with a difference from IFV of less than 0.2 *vu* at one site; 3) Unlikely – components with a BVS difference from IFV greater than 0.2 *vu* at one or more sites. All components, their probability and their assignment to certain categories are listed in Table 8.

The comparison of bond lengths and total Al revealed interesting differences between the series examined in natural tourmalines: 1) Tourmalines of the schorl-elbaite series show a very good correlation for all bond lengths; 2) Tourmalines of the elbaite-liddicoatite series have a longer *Y*-O2 due to ^{X}Ca, which is compensated by a shorter *Y*-O6, resulting in a decrease in the *Z*-O6 bond valence, an increase in the bond valence of *Z*-O3 and eventually in an elongation of the *Y*-O3 bond; 3) Natural rossmanite samples follow the trend of the theoretical oxy-components **2.2**, **2.3** and **2.4**, while ertlite with the extremely shortened *Y*-O6 distance is close to the oxy-component **1.3**.

Aluminium-rich tourmaline with varying amounts of Na^{1+} (different proportions of Na and vacancies at the *X* site) but without Ca can only contain a limited portion of Li (≤1 *apfu* ^{Y}Li) considering the possible short-range orders (Table 10). This is consistent with the different chemical compositions of synthetic, aluminium-rich tourmaline. Tourmaline with higher Li content (Li >1 *apfu*) can be synthesized if, for example, Ca^{2+} is present in the starting material. Such tourmaline requires fluorine, because more Li results in O1 underbonding, while more Al at the *Y* site leads to O1 overbonding, as was demonstrated by bond valence calculations. It was demonstrated that an underbonding of O1 is preferable for F

https://doi.org/10.1180/mgm.2025.28 Published online by Cambridge University Press

because OH at the O1 site (*W* site) usually has a bond valence sum (BVS) higher than 1.00 vu due to hydrogen bonding of H to ring oxygen atoms. Therefore, liddicoatitic tourmaline is enriched in F rather than OH and is usually F dominant. If fluorine is not available in the starting material of a tourmaline synthesis, either O or OH will occupy the *W* site. Most of the likely components with O or OH at the *W* site also contain B or Al at the *T* site of Al-rich tourmaline lacking Fe^{2+} or Mn^{2+} (Table 10). Therefore, it is likely that significant proportions of B and/or Al are incorporated into the tetrahedral position of such tourmaline samples. Ultimately, however, such samples contain, on average, only a smaller proportion of Li, especially if they do not contain Ca. It is also interesting that tourmaline samples with Ca, $^{[4]}$B or $^{[4]}$Al, and OH at the *W* site would be stable even if one of the three *Y* sites is vacant (**3.3**, **3.4**, Table 8). Therefore, for the synthesis of Al- and Li-rich tourmaline, we recommend that the starting material also contains (besides Na) also Ca and F.

Acknowledgements

This contribution is dedicated to celebrating the long and successful career of Edward S. Grew, who is our role model as a scientist, with his outstanding and long career, his attention to detail and perception of the wider picture at the same time. The authors would like to thank the editor and reviewers. This research was funded by the EU NextGenerationEU through the Recovery and Resilience Plan for Slovakia under the project No. 09I03-03-V04-00060 (PB) and by the Austrian Science Fund (FWF) project P 35585 (AE). For the purpose of open access, the author has applied a CC BY public copyright license to any Author Accepted Manuscript version arising from this submission.

https://doi.org/10.1180/mgm.2025.28 Published online by Cambridge University Press

Declaration of Competing Interest

All the authors declare that they are in no current or potential conflict of interest, including any financial, personal or other relationships with other people or organizations that could inappropriately influence, or be perceived to influence their work.

Author contribution:

PB: Conceptualization, Investigation, Data Curation, Formal analysis, Writing – Original Draft, Writing - Review & Editing; AE: Conceptualization, Investigation, Writing – Original Draft, Writing - Review & Editing

https://doi.org/10.1180/mgm.2025.28 Published online by Cambridge University Press

References

Bačík P. (2018) The crystal-chemical autopsy of octahedral sites in Na-dominant tourmalines: Octahedral metrics model unconstrained by the *Y*,*Z*-site disorder assignment. *Journal of Geosciences* (Czech Republic), **63**, 137–154.

Bačík P. (2025a) The bond-valence topological field modeling I: The bond-valence topological map of dravite from Forshammar, Sweden. *In prep*.

Bačík P. (2025b) The bond-valence topological field modeling II: The bond-valence topological fields and determination of structural effects on an example of tetrahedral substitutions in tourmaline-supergroup minerals. *In prep*.

Bačík P. and Fridrichová J. (2021) Cation partitioning among crystallographic sites based on bond-length constraints in tourmaline-supergroup minerals. *American Mineralogist*, **106**, 851–861.

Bačík P., Uher P., Ertl A., Jonsson E., Nysten P., Kanický V., Vaculovič T. (2012) Zoned REE-enriched dravite from a granitic pegmatite in Forshammar, Bergslagen Province, Sweden: An EMPA, XRD and LA-ICP-MS study. *The Canadian Mineralogist*, **50**, 825–841

Bosi F. (2010) Octahedrally coordinated vacancies in tourmaline: a theoretical approach. *Mineralogical Magazine*, **74**, 1037–1044.

Bosi F. (2011) Stereochemical constraints in tourmaline: from a short-range to a long-range structure. *The Canadian Mineralogist*, **49**, 17–27.

Bosi F. (2013) Bond-valence constraints around the O1 site of tourmaline. *Mineralogical Magazine*, **77**, 343–351.

Bosi F. (2018) Tourmaline crystal chemistry. *American Mineralogist*, **103**, 298–306.

Bosi F., Agrosi G., Lucchesi S., Melchiorre G., Scandale E. (2005a) Mn-tourmaline from island of Elba (Italy): Crystal chemistry. *American Mineralogist*, **90**, 1661–1668.

https://doi.org/10.1180/mgm.2025.28 Published online by Cambridge University Press

Bosi F., Andreozzi G.B., Federico M., Graziani G., Lucchesi S. (2005b) Crystal chemistry of the elbaite-schorl series. *American Mineralogist*, **90**, 1784–1792.

Bosi F., Skogby H., Agrosi G., Scandale E. (2012) Tsilaisite, $NaMn_3Al_6(Si_6O_{18})(BO_3)_3(OH)_3OH$, a new mineral species of the tourmaline supergroup from Grotta d'Oggi, San Pietro in Campo, island of Elba, Italy. *American Mineralogist*, **97**, 989–994.

Bosi F., Andreozzi G.B., Skogby H., Lussier A.J., Abdu Y., Hawthorne F.C. (2013) Fluor-elbaite, $Na(Li_{1.5}Al_{1.5})Al_6(Si_6O_{18})(BO_3)_3(OH)_3F$, a new mineral species of the tourmaline supergroup. *American Mineralogist*, **98**, 297–303.

Bosi F., Andreozzi G.B., Agrosi G., Scandale E. (2015) Fluor-tsilaisite, $NaMn_3Al_6(Si_6O_{18})(BO_3)_3(OH)_3F$, a new tourmaline from San Piero in Campo (Elba, Italy) and new data on tsilaisitic tourmaline from the holotype specimen locality. *Mineralogical Magazine*, **79**, 89–101.

Brown I.D. (2006) *The Chemical Bond in Inorganic Chemistry*. Oxford University Press, Oxford, UK, 292 pp.

Brown I.D. (2013) bvparm2013.cif.txt. http://www.iucr.org/resources/data/datasets/bond-valence-parameters (posted 16 October 2013)

Burns P.C., MacDonald D.J., Hawthorne F.C. (1994) The crystal chemistry of manganese-bearing elbaite. *The Canadian Mineralogist*, **32**, 31–41.

Cempírek J., Jonsson E., Skřápková L., Škoda R., Čopjaková R., Groat L.A., Kampf A.R., Lussier A.J., Hawthorne F.C., Haifler J. (2024) Ertlite, IMA 2023-086, in: CNMNC Newsletter 79, *European Journal of Mineralogy*, **36**, https://doi.org/10.5194/ejm-36-525-2024.

Ertl A. (2021): Why was it not possible to synthesize Li-rich tourmaline? *NATURA*, **111**, 31–32.

https://doi.org/10.1180/mgm.2025.28 Published online by Cambridge University Press

Ertl A. (2023): Are the [6]-coordinated sites in tourmaline in certain cases partially vacant? *Mineralogy and Petrology*, **117**, 201–207.

Ertl A. and Bačík P. (2020) Considerations About Bi and Pb in the Crystal Structure of Cu-Bearing Tourmaline. *Minerals*, **10**(8), 706.

Ertl A., Hughes J.M., Pertlik F., Foit F.F., Wright S.E., Brandstätter F., Marler B. (2002) Polyhedron distortions in tourmaline. *The Canadian Mineralogist*, **40**, 153–162.

Ertl A., Hughes J.M., Prowatke S., Ludwig T., Prasad P.S.R., Brandstätter F., Körner W., Schuster R., Pertlik F., Marschall H. (2006) Tetrahedrally coordinated boron in tourmalines from the liddicoatite-elbaite series from Madagascar: Structure, chemistry, and infrared spectroscopic studies. *American Mineralogist*, **91**, 1847–1856.

Ertl A., Hughes J.M., Prowatke S., Ludwig T., Brandstätter F., Körner W., Dyar M.D. (2007) Tetrahedrally-coordinated boron in Li-bearing olenite from "mushroom" tourmaline from

Momeik, Myanmar. *The Canadian Mineralogist*, **45**, 891–899.

Ertl A., Tillmanns E., Ntaflos T., Francis C., Giester G., Körner W., Hughes J.M., Lengauer C., Prem M. (2008) Tetrahedrally coordinated boron in Al-rich tourmaline and its relationship to the pressure–temperature conditions of formation. *European Journal of Mineralogy*, **20**, 881–888.

Ertl A., Rossman G., Hughes J.M., London D., Wang Y., O'Leary J.A., Darby M.D., Prowatke S., Ludwig T., Tillmanns E. (2010) Tourmaline of the elbaite-schorl series from the Himalaya Mine, Mesa Grande, California: A detailed investigation. *American Mineralogist*, **95**, 24–40.

Ertl A., Giester G., Ludwig T., Meyer H.-P., Rossman G.R. (2012a) Synthetic B-rich olenite: Correlations of single-crystal structural data. *American Mineralogist*, **97**, 1591–1597.

https://doi.org/10.1180/mgm.2025.28 Published online by Cambridge University Press

Ertl A., Hughes J.M., Prowatke S., Ludwig T., Lengauer C.L., Meyer H.-P., Giester G., Kolitsch U., Prayer A. (2022) Alumino-oxy-rossmanite from pegmatites in Variscan metamorphic rocks from Eibenstein an der Thaya, Lower Austria, Austria. *American Mineralogist*, **107**, 157–166.

Ertl A., Schuster R., Hughes J.M., Ludwig T., Meyer H.-P., Finger F., Dyar M.D., Ruschel K., Rossman G..R., Klotzli U., Brandstatter F., Lengauer C.L., Tillmanns E. (2012b) Li-bearing tourmalines in Variscan granitic pegmatites from the Moldanubian nappes, Lower Austria. *European Journal of Mineralogy*, **24**, 695–715.

Ertl A., Kolitsch U., Dyar M.D., Hughes J.M., Rossman G.R., Pieczka A., Henry D.J., Pezzotta F., Prowatke S., Lengauer C.L., Korner W., Brandstatter F., Francis C.A., Prem M., Tillmanns E. (2012) Limitations of Fe^{2+} and Mn^{2+} site occupancy in tourmaline: Evidence from Fe^{2+}- and Mn^{2+}-rich tourmaline. *American Mineralogist*, **97** 1402–1416.

Gagné O.C. and Hawthorne F.C. (2015) Comprehensive derivation of bond-valence parameters for ion pairs involving oxygen. *Acta Crystallographica Section B: Structural Science, Crystal Engineering and Materials*, **71**, 562–578.

Gatta G.D., Danisi R.M., Adamo I., Meven M., Diella V. (2012) A single-crystal neutron and X-ray diffraction study of elbaite. *Physics and Chemistry of Minerals*, **39**, 577–588.

Gatta G.D., Bosi F., McIntyre G.J., Skogby H. (2014) First accurate location of two proton sites in tourmaline: A single-crystal neutron diffraction study of oxy-dravite. *Mineralogical Magazine*, **78**, 681–692

Hawthorne F.C. (1996) Structural mechanisms for light-element variations in tourmaline. *The Canadian Mineralogist*, **34**, 123–132.

Hawthorne F.C. (2002) Bond-valence constraints on the chemical composition of tourmaline. *The Canadian Mineralogist*, **40**, 789–797.

https://doi.org/10.1180/mgm.2025.28 Published online by Cambridge University Press

Hellingwerf, R.H., Gatedal, K., Gallagher, V., Baker, J.H. (1994) Tourmaline in the central Swedish ore district. *Mineralium Deposita*, **29**, 189–205.

Henry D.J. and Dutrow B.L. (2011) The incorporation of fluorine in tourmaline: internal crystallographic controls or external environmental influences? *The Canadian Mineralogist*, **49**, 41–56

Henry D.J., Novák M., Hawthorne F.C., Ertl A., Dutrow B.L., Uher P., Pezzotta F. (2011) Nomenclature of the tourmaline-supergroup minerals. *American Mineralogist*, **96**, 895–913.

Kasatkin A.V., Nestola F., Day M.C., Gorelova L.A., Škoda R., Vereshchagin O.S., Agakhanov A.A., Belakovskiy D.I., Pamato M.G., Cempírek J. (2024) Fluor-rossmanite, $\square(Al_2Li)Al_6(Si_6O_{18})(BO_3)_3(OH)_3F$, a new tourmaline supergroup mineral from Malkhan pegmatite field, Western Siberia, Russia. *Mineralogical Magazine*, Published online 2024:1-9. doi:10.1180/mgm.2024.34.

Lussier A.J., Abdu Y., Hawthorne F.C., Michaelis V.K., Aguiar P.M., Kroeker S. (2011) Oscillatory zoned liddicoatite from Anjanabonoina, central Madagascar. I. Crystal chemistry and structure by SREF and ^{11}B and ^{27}Al MAS NMR spectroscopy. *The Canadian Mineralogist*, **49**, 63–88.

Novák, M., Škoda, R., Filip, J., Macek, I., Vaculovič, T. (2011) Compositional trends in tourmaline from intragranitic NYF pegmatites of the Třebíč Pluton, Czech Republic: an electron microprobe, Mössbauer and LA–ICP–MS study. *The Canadian Mineralogist*, **49**, 359–380.

Rieder M., Cavazzini G., Yakonov Y.S., Frank-Kamenetskii V.A., Gottardi G., Guggenheim S., Koval P.V., Müller G., Neiva A.M.R., Radoslovich E.W., Robert J.-L., Sassi F.P., Takeda H., Weiss Z., Wones D.R. (1999) Nomenclature of the micas. *Mineralogical Magazine*, **63**, 267-279.

https://doi.org/10.1180/mgm.2025.28 Published online by Cambridge University Press

Selway JB, Novák M, Hawthorne FC, Černý P, Ottolini L, Kyser TK (1998): Rossmanite, $\square(LiAl_2)Al_6Si_6O_{18}(BO_3)_3(OH)_4$, a new alkali-deficient tourmaline: description and crystal structure. *American Mineralogist*, **83**, 896–900.

Vereshchagin O.S., Rozhdestvenskaya I.V., Frank-Kamenetskaya O.V., Zolotarev A.A., Mashkovtsev R.I. (2013) Crystal chemistry of Cu-bearing tourmalines. *American Mineralogist*, **98**, 1610–1616.

https://doi.org/10.1180/mgm.2025.28 Published online by Cambridge University Press

Figure captions:

Fig. 1. Detail of the crystal structure of tourmaline with the purple circle surrounding the studied part of the structure.

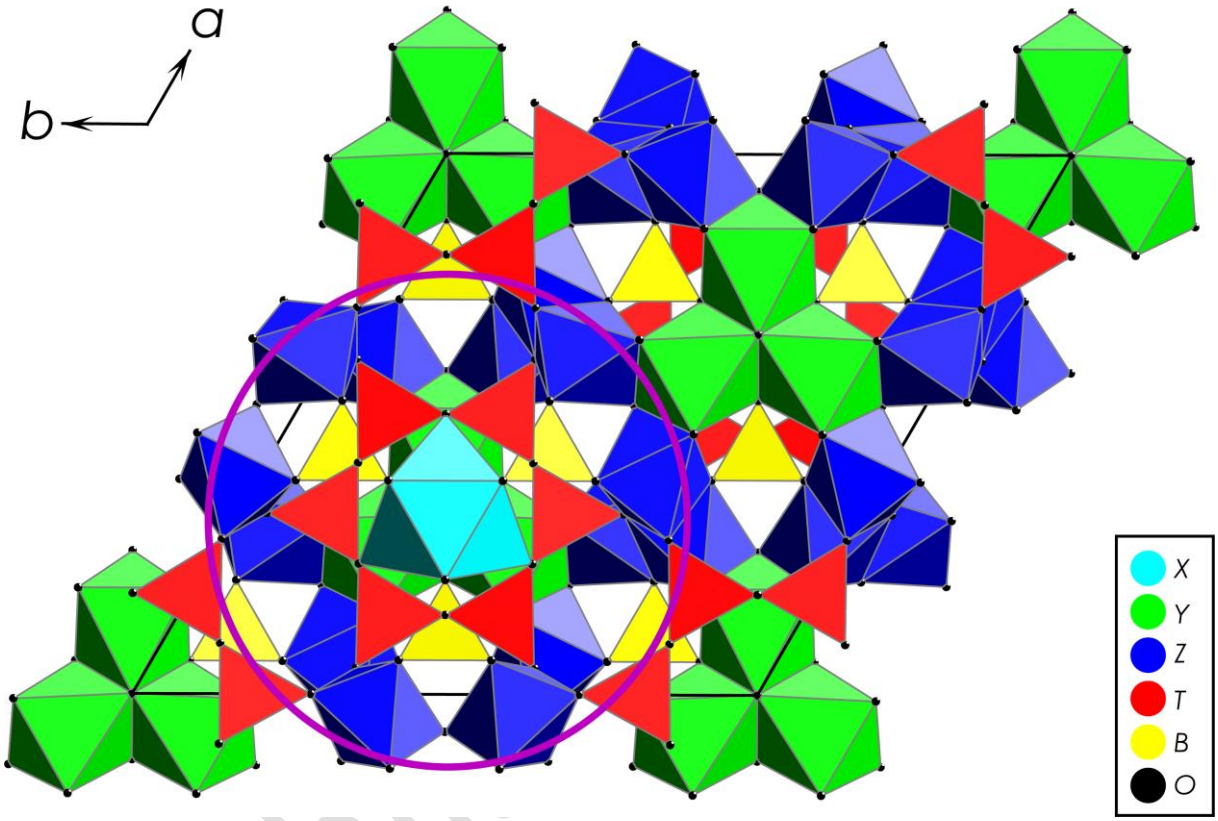

https://doi.org/10.1180/mgm.2025.28 Published online by Cambridge University Press

Fig. 2. Planar bond-topological graph of tourmaline structure segment encircled in Fig. 1. Transformation of 3D structure to the planar graph was not fully possible, but the spatial relationship is highlighted by the lines used. Full lines are bonds in the plane of the graph, dashed lines are for bonds below, and dash-dotted lines are for bonds above the plane. Dotted lines connect sites, which are identical, but in order to maintain readability of the graph and keep the local environment (i.e. to keep octahedra easily recognisable), were displayed at two or more places. Note that the *X* site in the middle of the graph is different to one on the surrounding circle.

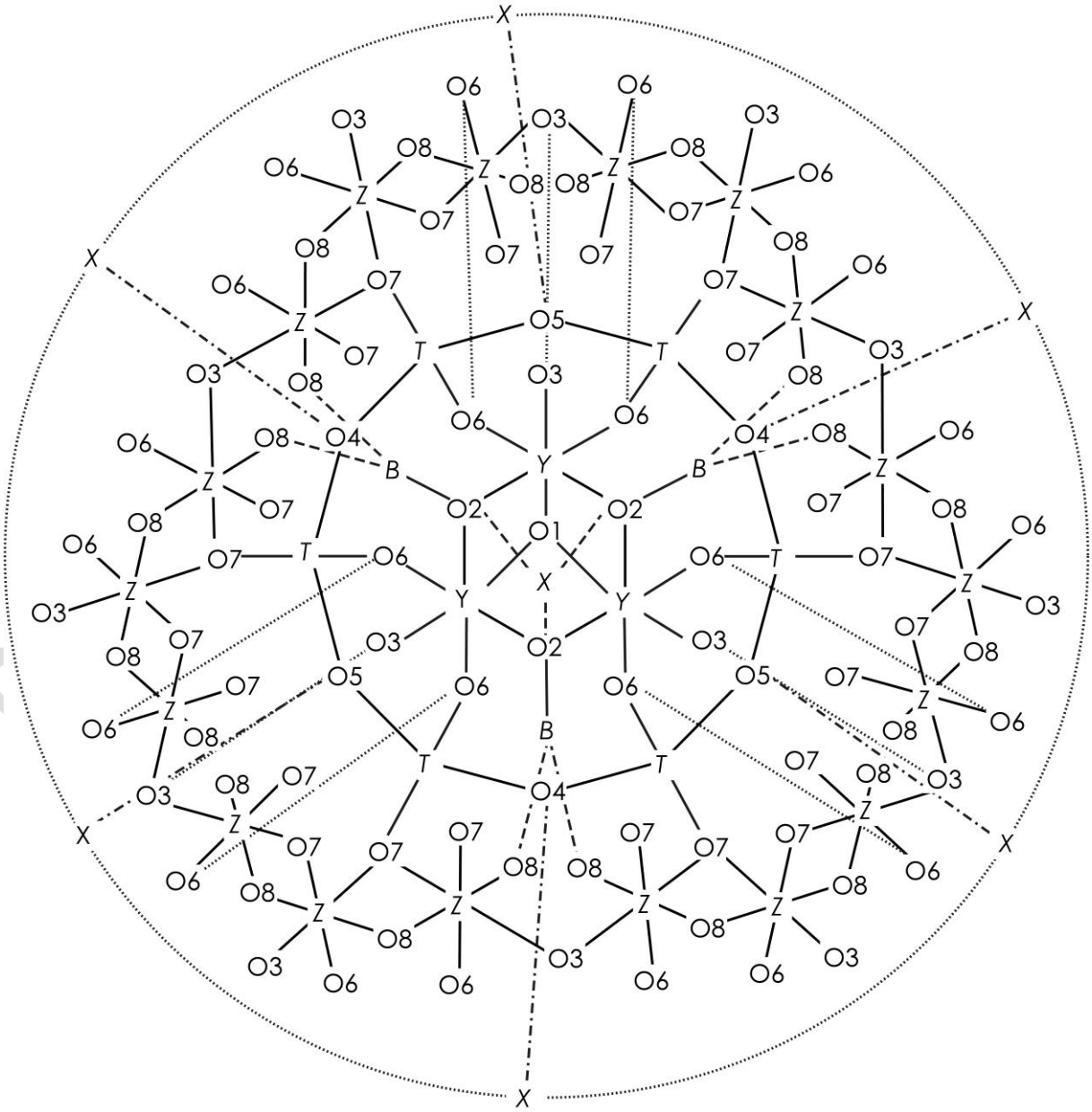

https://doi.org/10.1180/mgm.2025.28 Published online by Cambridge University Press

Fig. 3. The comparison of total Al content to each bond length (in Å; **a** – *Y*-O1; **b** – *Y*-O2; **c** – *Y*-O3; **d** – *Y*-O4) and their sums (**e** – O1-*Y*-O3; **f** – O2-*Y*-O6).

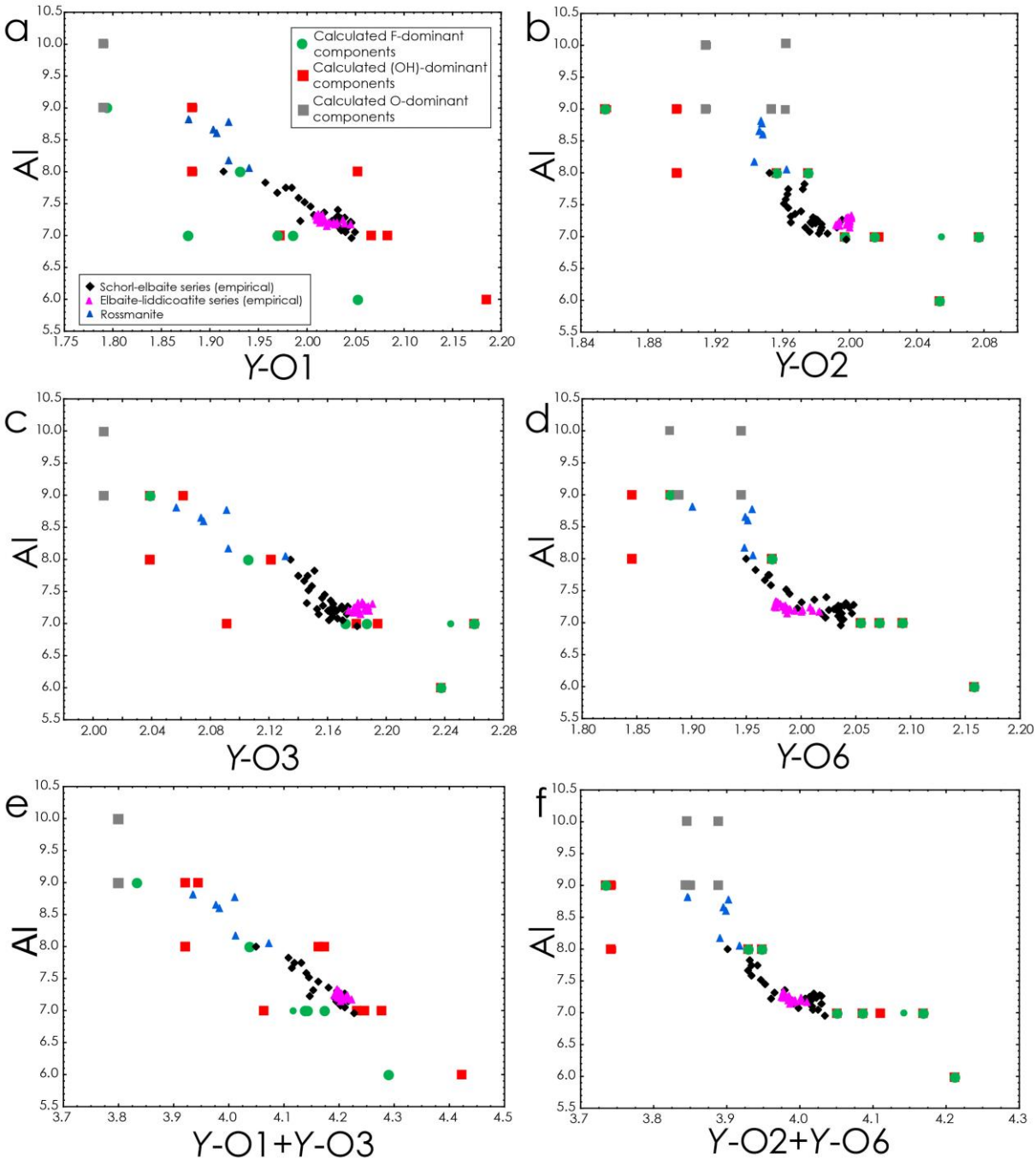

https://doi.org/10.1180/mgm.2025.28 Published online by Cambridge University Press

Table 1. Natural (N), synthetic (S) and alternative (A) theoretical components with variable short-range ordering schemes.

Number	*X* site	*Y* site	*T* site	*W* site	*Type*
0.1	Na	$AlLiMn^{2+}$	Si_6	OH	A
0.2	Na	$AlLiFe^{2+}$	Si_6	OH	A
0.3	Na	$AlLiMn^{2+}$	Si_6	F	A
0.4	Na	$AlLiFe^{2+}$	Si_6	F	A
1.1	Na	Al_2Li	Si_5B	OH	S
1.2	Na	Al_2Li	Si_5Al	OH	S
1.3	Na	Al_3	Si_4B_2	O	S
1.3a	Na	Al_3	Si_4B_2	OH	A
1.3b	Na	Al_3	Si_4B_2	F	A
1.4	Na	Al_2Li	Si_5B	F	N
1.5	Na	Al_2Li	Si_5Al	F	N
1.6	Na	$Al_2□$	Si_6	OH	A
1.7	Na	Li_2Al	Si_6	F	A
1.8	Na	Li_2Al	Si_6	OH	A
1.9	Na	Li_3	Si_6	OH	A
1.10	Na	Li_3	Si_6	F	A
2.1	□	Al_2Li	Si_6	OH	S
2.2	□	Al_3	Si_5B	O	S
2.3	□	Al_3	Si_5Al	O	S
2.4	□	Al_2Li	Si_6	F	N
3.1	Ca	Li_2Al	Si_6	F	N
3.2	Ca	Li_2Al	Si_6	OH	N
3.3	Ca	$Al_2□$	Si_5Al	OH	N
3.4	Ca	$Al_2□$	Si_5B	OH	N

https://doi.org/10.1180/mgm.2025.28 Published online by Cambridge University Press

Table 2. Calculated bond valence sums for *T*, *Y*, *X* and O1-O8 sites in ^{W}OH-bearing components and their difference to **0.1** component. Values in bold are significantly different to the ideal formal valence of ion at specific site.

	X	Na	a	iff.	a	iff.	a	iff.	a	iff.	a	iff.	a	iff.	a	iff.		iff.	a	iff.	a	iff.	a	iff.
	Y	AlMnLi	lFeLi		l_2Li		l_2Li		l_3		l_2□		i_2Al		i_3		l_2Li		i_2Al		l_2□		l_2□	
	T	Si$_6$	i$_6$		i$_5$B		i$_5$Al		i$_4$B$_2$		i$_6$		i$_6$		i$_6$		i$_6$		i$_6$		i$_5$Al		i$_5$B	
	W	OH	H		H		H		H		H		H		H		H		H		H		H	
Component		**0.1**	**.2**		**.1**		**.2**		**.3a**		**.6**		**.8**		**.9**		**.1**		**.2**		**.3**		**.4**	
	***T*1**	4.050	.050	.000	.950	1.100	.950	1.100	.950	1.100	.040	0.010	.050	.000	.050	.000	.050	.000	.040	0.010	.950	1.100	.950	1.100
	***T*2**	4.050	.050	.000	.050	.000	.050	.000	.050	.000	.040	0.010	.050	.000	.050	.000	.050	.000	.040	0.010	.040	0.010	.040	0.010
	***T*3**	4.050	.050	.000	.050	.000	.050	.000	.050	.000	.040	0.010	.050	.000	.050	.000	.050	.000	.040	0.010	.040	0.010	.040	0.010
	***T*4**	4.050	.050	.000	.050	.000	.050	.000	.950	1.100	.040	0.010	.050	.000	.050	.000	.050	.000	.040	0.010	.040	0.010	.040	0.010
	***T*5**	4.050	.050	.000	.050	.000	.050	.000	.050	.000	.040	0.010	.050	.000	.050	.000	.050	.000	.040	0.010	.040	0.010	.040	0.010
	***T*6**	4.050	.050	.000	.050	.000	.050	.000	.050	.000	.040	0.010	.050	.000	.050	.000	.050	.000	.040	0.010	.040	0.010	.040	0.010
T	**Av.**	4.050	.050	.000	.867	0.183	.867	0.183	.683	0.367	.040	0.010	.050	.000	.050	.000	.050	.000	.040	0.010	.858	0.192	.858	0.192
	***Y*1**	2.100	.100	.000	.996	.896	.996	.896	.056	.956	.066	.966	**.156**	**.056**	.125	0.975	.076	.976	**.166**	**.066**	.066	.966	.006	.906
	***Y*2**	3.056	.056	.000	.996	0.060	.996	0.060	.056	.000	.066	.010	.035	2.021	.125	1.871	.076	.020	.145	1.911	.066	.010	.006	.010
	***Y*3**	1.125	.125	.000	.995	0.130	.995	0.130	.056	.931	.000	1.125	.035	0.090	.125	.000	.995	0.130	.145	.020	.000	1.125	.000	1.125
Y	**Av.**	2.094	.094	.000	.329	.235	.329	.235	.056	.962	.044	0.050	.742	0.352	.125	0.949	.396	.302	.819	0.275	.044	0.050	.004	0.070
	X	0.904	.904	.000	.996	.896	.996	.896	.904	.000	.904	.000	.904	.000	.904	.000	.000	0.904	.932	.028	.892	.988	.892	.988
X+Y+T		3.43	1.43		1.22		1.22		1.99		1.16		0.45		8.58		1.38		1.38		1.06		1.06	
	O1	1.051	.051	.000	.051	.000	.051	.000	**.585**	**.534**	.057	.006	.057	.006	**.523**	**0.528**	.051	.000	.057	.006	.057	.006	.057	.006
	O2	1.951	.951	.000	.017	.066	.017	.066	**.305**	**.355**	.855	0.096	**.782**	**0.169**	**.600**	**0.331**	.917	0.033	.003	.052	.044	.094	.004	.074
	O3	1.143	.143	.000	.081	0.062	.081	0.062	.163	.020	.139	0.005	.131	0.013	.120	0.024	.081	0.062	.147	.003	.139	0.005	.139	0.005

https://doi.org/10.1180/mgm.2025.28 Published online by Cambridge University Press

O4	2.066	.066	.000	.007	0.060	.007	0.060	.947	0.119	.056	0.010	.066	.000	.066	.000	.997	0.069	.118	.052	.060	0.006	.060	0.006
O5	1.999	.999	.000	.925	0.073	.925	0.073	.852	0.146	.989	0.010	.999	.000	.999	.000	.919	0.079	.067	.068	.995	0.004	.995	0.004
O6	1.993	.993	.000	.987	0.006	.987	0.006	.000	.007	.004	.011	.971	0.022	.935	0.058	.013	.020	.971	0.022	.978	0.015	.978	0.015
O7	2.036	.036	.000	.026	0.010	.026	0.010	.016	0.020	.036	.000	.036	.000	.036	.000	.036	.000	.036	.000	.026	0.010	.026	0.010
O8	2.022	.022	.000	.022	.000	.022	.000	.022	.000	.022	.000	.022	.000	.022	.000	.022	.000	.022	.000	.022	.000	.022	.000

https://doi.org/10.1180/mgm.2025.28 Published online by Cambridge University Press

Table 3. Calculated bond valence sums for *T*, *Y*, *X* and O1-O8 sites in ^{W}F-bearing components and their difference to **0.3** component. Values in bold are significantly different to the ideal formal valence of ion at specific site.

	X	**Na**	**diff.**	**Na**	**diff.**	**Na**	**diff.**	**Na**	**diff.**	**Na**	**diff.**	**Na**	**diff.**	**Na**	**diff.**	**□**	**diff.**	**Ca**	**diff.**
	Y	**AlMnLi**		**AlFeLi**		**Al$_2$Li**		**Al$_2$Li**		**Al$_3$**		**Li$_2$Al**		**Li$_3$**		**Al$_2$Li**		**Li$_2$Al**	
	T	**Si$_6$**		**Si$_6$**		**Si$_5$B**		**Si$_5$Al**		**Si$_4$B$_2$**		**Si$_6$**		**Si$_6$**		**Si$_6$**		**Si$_6$**	
	W	**F**		**F**		**F**		**F**		**F**		**F**		**F**		**F**		**F**	
t	**Component**	**0.3**		**0.4**		**1.4**		**1.5**		**1.3b**		**1.7**		**1.10**		**2.4**		**3.1**	
	***T*1**	4.050	0.000	4.050	0.000	2.950	-1.100	2.950	-1.100	2.950	-1.100	4.050	0.000	4.050	0.000	4.050	0.000	4.050	0.000
	***T*2**	4.050	0.000	4.050	0.000	4.050	0.000	4.050	0.000	4.050	0.000	4.050	0.000	4.050	0.000	4.050	0.000	4.050	0.000
	***T*3**	4.050	0.000	4.050	0.000	4.050	0.000	4.050	0.000	4.050	0.000	4.050	0.000	4.050	0.000	4.050	0.000	4.050	0.000
	***T*4**	4.050	0.000	4.050	0.000	4.050	0.000	4.050	0.000	2.950	-1.100	4.050	0.000	4.050	0.000	4.050	0.000	4.050	0.000
	***T*5**	4.050	0.000	4.050	0.000	4.050	0.000	4.050	0.000	4.050	0.000	4.050	0.000	4.050	0.000	4.050	0.000	4.050	0.000
	***T*6**	4.050	0.000	4.050	0.000	4.050	0.000	4.050	0.000	4.050	0.000	4.050	0.000	4.050	0.000	4.050	0.000	4.050	0.000
	Average *T*	4.050	0.000	4.050	0.000	3.867	-0.183	3.867	-0.183	3.683	-0.367	4.050	0.000	4.050	0.000	4.050	0.000	4.050	0.000
	***Y*1**	2.080	0.000	2.080	0.000	2.976	-0.896	2.976	-0.896	3.056	-0.976	**3.119**	**-0.039**	1.105	-0.975	3.056	-0.976	3.079	-0.999
	***Y*2**	3.056	0.000	3.056	0.000	2.976	-0.080	2.976	-0.080	3.056	0.000	1.025	2.031	1.084	1.912	3.056	0.000	1.025	2.031
	***Y*3**	1.105	0.000	1.105	0.000	0.995	-0.110	0.995	-0.110	3.056	1.951	1.025	-0.080	1.105	0.000	0.995	-0.110	1.025	-0.080
	Average *Y*	2.080	0.000	2.080	0.000	2.316	-0.235	2.316	-0.235	3.056	0.976	1.723	1.723	1.098	-0.962	2.369	-0.289	1.710	-0.371
	X	0.904	0.000	0.904	0.000	0.904	0.000	0.904	0.000	0.904	0.000	0.904	0.904	0.904	0.000	0.000	-0.904	1.962	1.058
	X+Y+T	31.39		31.39		31.20		31.20		31.99		30.39		28.45		31.38		31.34	
	O1	0.991	0.000	0.991	0.000	1.001	0.010	1.001	0.010	1.525	0.534	1.000	0.009	**0.463**	**-0.528**	1.001	0.010	1.000	0.009

https://doi.org/10.1180/mgm.2025.28 Published online by Cambridge University Press

O2	1.9	0	1.	0	2	0	2	0	**2**	**0**	**1**	**-**	**1**	**-**	1	-	2	0
	51	.000	951	.000	.017	.066	.017	.066	**.305**	**.355**	**.782**	**0.169**	**.600**	**0.331**	.917	0.033	.001	.051
O3	1.1	0	1.	0	1	0	1	0	1	0	1	-	1	-	1	0	1	-
	45	.000	145	.000	.157	.012	.157	.012	.168	.023	.131	0.014	.120	0.025	.157	.012	.134	0.011
O4	2.0	0	2.	0	2	-	2	-	1	-	2	0	2	0	1	-	2	0
	66	.000	066	.000	.007	0.060	.007	0.060	.947	0.119	.066	.000	.066	.000	.997	0.069	.128	.062
O5	1.9	0	1.	0	1	-	1	-	1	-	1	0	1	0	1	-	2	0
	99	.000	999	.000	.925	0.073	.925	0.073	.852	0.146	.999	.000	.999	.000	.919	0.079	.077	.078
O6	1.9	0	1.	0	1	-	1	-	2	0	1	-	1	-	2	0	1	-
	93	.000	993	.000	.987	0.006	.987	0.006	.000	.007	.971	0.022	.934	0.059	.013	.020	.971	0.022
O7	2.0	0	2.	0	2	-	2	-	2	-	2	0	2	0	2	0	2	0
	36	.000	036	.000	.026	0.010	.026	0.010	.016	0.020	.036	.000	.036	.000	.036	.000	.036	.000
O8	2.0	0	2.	0	2	0	2	0	2	0	2	0	2	0	2	0	2	0
	21	.000	021	.000	.021	.000	.021	.000	.021	.000	.021	.000	.021	.000	.021	.000	.021	.000

https://doi.org/10.1180/mgm.2025.28 Published online by Cambridge University Press

Table 4. Calculated bond valence sums for *T*, *Y*, *X* and O1-O8 sites in ^{W}O-bearing components and their difference to **0.1** component.

	X	**a**	**iff.**		**iff.**		**iff.**
	Y	**l_3**		**l_3**		**l_3**	
	T	**i_4B_2**		**i_5B**		**i_5Al**	
	W						
Component		**.3**		**.2**		**.3**	
	***T*1**	.950	1.100	.950	1.100	.950	1.100
	***T*2**	.050	.000	.050	.000	.050	.000
	***T*3**	.050	.000	.050	.000	.050	.000
	***T*4**	.950	1.100	.050	.000	.050	.000
	***T*5**	.050	.000	.050	.000	.050	.000
	***T*6**	.050	.000	.050	.000	.050	.000
Average *T*		.683	0.367	.867	0.183	.867	0.183
	***Y*1**	.972	.872	.923	.823	.923	.823
	***Y*2**	.972	0.024	.923	0.073	.923	0.073
	***Y*3**	.972	.847	.923	.798	.923	.798
Average *Y*		.972	.899	.923	.849	.923	.849
	X	.028	.124				
X*+*Y*+*T		2.05		2.47		2.47	
	O1	.000	.949	.995	.944	.995	.944
	O2	.021	.090	.992	.062	.992	.062

https://doi.org/10.1180/mgm.2025.28 Published online by Cambridge University Press

O3	.150	.004	.150	.004	.150	.004
O4	.976	0.090	.938	0.129	.938	0.129
O5	.897	0.101	.846	0.153	.846	0.153
O6	.997	.004	.005	.012	.005	.012
O7	.016	0.020	.026	0.010	.026	0.010
O8	.022	.000	.022	.000	.022	.000

https://doi.org/10.1180/mgm.2025.28 Published online by Cambridge University Press

Table 5. Bond lengths (Å) at *T*, *Y*, and *X* sites in ^{W}OH-bearing components calculated from BVS in Table 4 and their difference to **0.3** order.

	X	Na	a	iff.	a	iff.	a	iff.	a	iff.	a	iff.	a	iff.	a	iff.		iff.	a	iff.	a	iff.	a	iff.
	Y	AlMnLi	lFeLi		l_2Li		l_2Li		l_3		l_2□		i_2Al		i_3		l_2Li		i_2Al		l_2□		l_2□	
	T	Si$_6$	i$_6$		i_5B		i_5Al		i_4B_2		i$_6$		i$_6$		i$_6$		i$_6$		i$_6$		i_5Al		i_5B	
	W	OH	H		H		H		H		H		H		H		H		H		H		H	
Component		**0.1**	**.2**		**.1**		**.2**		**.3a**		**.6**		**.8**		**.9**		**.1**		**.2**		**.3**		**.4**	
	***T*-O4**	1.6245	.6245	.0000	.5942	0.0303	.6390	.0145	.5639	0.0606	.6265	.0020	.6245	.0000	.6245	.0000	.6245	.0000	.6265	.0020	.6406	.0161	.5959	0.0286
	***T*-O5**	1.6400	.6400	.0000	.6132	0.0268	.6586	.0186	.5865	0.0535	.6420	.0020	.6400	.0000	.6400	.0000	.6400	.0000	.6420	.0020	.6603	.0203	.6149	0.0251
	***T*-O6**	1.6065	.6065	.0000	.5998	0.0067	.6465	.0400	.5932	0.0133	.6065	.0000	.6065	.0000	.6065	.0000	.6065	.0000	.6065	.0000	.6465	.0400	.5998	0.0067
	***T*-O7**	1.6066	.6066	.0000	.5800	0.0266	.6249	.0183	.5535	0.0531	.6066	.0000	.6066	.0000	.6066	.0000	.6066	.0000	.6066	.0000	.6249	.0183	.5800	0.0266
O>	**<*T*-**	1.6194	.6194	.0000	.5968	0.0226	.6422	.0228	.5743	0.0451	.6204	.0010	.6194	.0000	.6194	.0000	.6194	.0000	.6204	.0010	.6431	.0237	.5977	0.0217
	***Y*-O1**	2.0822	.0654	0.0168	.0519	0.0303	.0519	0.0303	.8828	0.1994	.8828	0.1994	.9725	0.1097	.1838	.1016	.0519	0.0303	.9725	0.1097	.8828	0.1994	.8828	0.1994
	***Y*-O2**	2.0150	.9972	0.0178	.9754	0.0397	.9754	0.0397	.8558	0.1592	.8979	0.1171	.0762	.0611	.0532	.0311	.9570	0.0581	.0175	.0024	.8979	0.1171	.8979	0.1171
	***Y*-O2**	2.0150	.9972	0.0178	.9754	0.0397	.9754	0.0397	.8558	0.1592	.8979	0.1171	.0762	.0611	.0532	.0311	.9570	0.0581	.0175	.0024	.8979	0.1171	.8979	0.1171
	***Y*-O3**	2.1944	.1801	0.0143	.1219	0.0724	.1219	0.0724	.0622	0.1322	.0395	0.1549	.2601	.0657	.2373	.0430	.1219	0.0724	.0916	0.1028	.0395	0.1549	.0395	0.1549
	***Y*-O6**	2.0704	.0535	0.0169	.9728	0.0976	.9728	0.0976	.8809	0.1895	.8458	0.2246	.0913	.0209	.1565	.0861	.9728	0.0976	.0913	.0209	.8458	0.2246	.8458	0.2246
	***Y*-O6**	2.0704	.0535	0.0169	.9728	0.0976	.9728	0.0976	.8809	0.1895	.8458	0.2246	.0913	.0209	.1565	.0861	.9728	0.0976	.0913	.0209	.8458	0.2246	.8458	0.2246
O>	**<*Y*-**	2.0746	.0578	0.0168	.0117	0.0629	.0117	0.0629	.9031	0.1715	.9016	0.1729	.0946	.0200	.1401	.0632	.0056	0.0690	.0469	0.0276	.9016	0.1729	.9016	0.1729
	***X*-O2**	2.4865	.4865	.0000	.4865	.0000	.4865	.0000	.4865	.0000	.4865	.0000	.4865	.0000	.4865	.0000			.3238	0.1627	.3867	0.0998	.3867	0.0998
	***X*-O4**	2.8177	.8177	.0000	.8177	.0000	.8177	.0000	.8177	.0000	.8177	.0000	.8177	.0000	.8177	.0000			.7390	0.0787	.7390	0.0787	.7390	0.0787
	***X*-O5**	2.7595	.7595	.0000	.7595	.0000	.7595	.0000	.7595	.0000	.7595	.0000	.7595	.0000	.7595	.0000			.6634	0.0961	.6634	0.0961	.6634	0.0961
O>	**<*X*-**	2.6879	.6879	.0000	.6879	.0000	.6879	.0000	.6879	.0000	.6879	.0000	.6879	.0000	.6879	.0000			.5754	0.1125	.5964	0.0915	.5964	0.0915

https://doi.org/10.1180/mgm.2025.28 Published online by Cambridge University Press

https://doi.org/10.1180/mgm.2025.28 Published online by Cambridge University Press

Table 6. Bond lengths (Å) at *T*, *Y*, and *X* sites in ^{W}F-bearing components calculated from BVS in Table 4 and their difference to **0.1** component.

	X	**Na**	**Na**	**diff.**	**Na**	**diff.**	**Na**	**diff.**	**Na**	**diff.**	**Na**	**diff.**	**Na**	**diff.**		**diff.**	**Ca**	**diff.**
	Y	**AlMnLiS**	**AlFeLiS**		**l_3S**		**l_2LiS**		**l_2LiS**		**i_2AlS**		**i_3S**		**l_2LiS**		**i_2AlS**	
	T	**i_6**	**i_6**		**i_4B_2**		**i_5B**		**i_5Al**		**i_6**		**i_6**		**i_6**		**i_6**	
	W	**F**	**F**		**I**		**I**		**I**		**I**		**I**		**I**		**I**	
Component		**0.3**	**0.4**		**.3b**		**.4**		**.5**		**.7**		**.10**		**.1a**		**.1**	
	***T*-O4**	1.6245	1.6245	0.0000	1.5639	0.0606	1.5942	0.0303	1.6390	0.0145	1.6245	0.0000	1.6245	0.0000	1.6245	0.0000	1.6245	0.0000
	***T*-O5**	1.6400	1.6400	0.0000	1.5865	0.0535	1.6132	0.0268	1.6586	0.0186	1.6400	0.0000	1.6400	0.0000	1.6400	0.0000	1.6400	0.0000
	***T*-O6**	1.6065	1.6065	0.0000	1.5932	0.0133	1.5998	0.0067	1.6465	0.0400	1.6065	0.0000	1.6065	0.0000	1.6065	0.0000	1.6065	0.0000
	***T*-O7**	1.6066	1.6066	0.0000	1.5535	0.0531	1.5800	0.0266	1.6249	0.0183	1.6066	0.0000	1.6066	0.0000	1.6066	0.0000	1.6066	0.0000
O>	**<*T*-**	1.6194	1.6194	0.0000	1.5743	0.0451	1.5968	0.0226	1.6422	0.0228	1.6194	0.0000	1.6194	0.0000	1.6194	0.0000	1.6194	0.0000
	***Y*-O1**	1.9857	1.9697	0.0160	1.7953	0.1904	1.9312	0.0545	1.9312	0.0545	1.8783	0.1075	2.0516	0.0659	1.9312	0.0545	1.8783	0.1075
	***Y*-O2**	2.0150	1.9972	0.0178	1.8558	0.1592	1.9754	0.0397	1.9754	0.0397	1.9762	0.0611	2.0532	0.0311	1.9570	0.0581	1.9545	0.0395
	***Y*-O2**	2.0150	1.9972	0.0178	1.8558	0.1592	1.9754	0.0397	1.9754	0.0397	1.9762	0.0611	2.0532	0.0311	1.9570	0.0581	1.9545	0.0395
	***Y*-O3**	2.1868	2.1725	0.0143	2.0395	0.1473	2.1061	0.0807	2.1061	0.0807	2.2601	0.0733	2.2373	0.0506	2.1061	0.0807	2.2461	0.0594
	***Y*-O6**	2.0704	2.0535	0.0169	1.8809	0.1895	1.9728	0.0976	1.9728	0.0976	1.9913	0.0209	2.1565	0.0861	1.9728	0.0976	1.9913	0.0209
	***Y*-O6**	2.0704	2.0535	0.0169	1.8809	0.1895	1.9728	0.0976	1.9728	0.0976	1.9913	0.0209	2.1835	0.1130	1.9728	0.0976	1.9913	0.0209
O>	**<*Y*-**	2.0572	2.0406	0.0166	1.8847	0.1725	1.9889	0.0683	1.9889	0.0683	1.9789	0.0217	2.1226	0.0630	1.9828	0.0744	1.9694	0.0121
O2	***X*-**	2.4865	2.4865	0.0000	2.4865	0.0000	2.4865	0.0000	2.4865	0.0000	2.4865	0.0000	2.4865	0.0000			2.3182	0.1683
O4	***X*-**	2.8177	2.8177	0.0000	2.8177	0.0000	2.8177	0.0000	2.8177	0.0000	2.8177	0.0000	2.8177	0.0000			2.7390	0.0787
O5	***X*-**	2.7595	2.7595	0.0000	2.7595	0.0000	2.7595	0.0000	2.7595	0.0000	2.7595	0.0000	2.7595	0.0000			2.6634	0.0961
	<*X*-	2	2	0	2	0	2	0	2	0	2	0	2	0			2	-

https://doi.org/10.1180/mgm.2025.28 Published online by Cambridge University Press

O>	.6879	.6879	.0000	.6879	.0000	.6879	.0000	.6879	.0000	.6879	.0000	.6879	.0000		.5735	0.1144

https://doi.org/10.1180/mgm.2025.28 Published online by Cambridge University Press

Table 7. Bond lengths (Å) at *T*, *Y*, and *X* sites in ^{W}O-bearing components calculated from BVS in Table 4 and their difference to **0.1** component.

	X	**a**	**diff.**	**□**	**diff.**	**□**	**diff.**
	Y	**l_3**		**l_3**		**l_3**	
	T	**i_4B_2**		**i_5B**		**i_5Al**	
	W	**(**		**(**		**(**	
ponent	**Com**	**.3**		**.2**		**.3**	
O4	***T*-**	.5639	0.0606	.5942	0.0303	.6390	.0145
O5	***T*-**	.5865	0.0535	.6132	0.0268	.6586	.0186
O6	***T*-**	.5932	0.0133	.5998	0.0067	.6465	.0400
O7	***T*-**	.5535	0.0531	.5800	0.0266	.6249	.0183
O>	**<*T*-**	.5743	0.0451	.5968	0.0226	.6422	.0228
O1	***Y*-**	.7921	0.2900	.7931	0.2891	.7931	0.2891
O2	***Y*-**	.9540	0.0681	.9152	0.1069	.9152	0.1069
O2	***Y*-**	.9540	0.0681	.9152	0.1069	.9152	0.1069
O3	***Y*-**	.0077	0.1866	.0077	0.1866	.0077	0.1866
O6	***Y*-**	.8884	0.1820	.9446	0.1258	.9446	0.1258
O6	***Y*-**	.8884	0.1820	.9446	0.1258	.9446	0.1258
O>	**<*Y*-**	.9141	0.1628	.9201	0.1568	.9201	0.1568
O2	***X*-**	.5844	.0979				
O4	***X*-**	.6708	0.1469				
O5	***X*-**	.5707	0.1888				
	<*X*-		-				

https://doi.org/10.1180/mgm.2025.28 Published online by Cambridge University Press

O>	.6087	0.0792

https://doi.org/10.1180/mgm.2025.28 Published online by Cambridge University Press

Table 8 . The likelihood of studied theoretical components based on the bond-valence constraints: 1) Likely – BVS to IFV has a difference of less than 0.1 *vu*; 2) Reasonable – BVS to IFV with difference of more than 0.1 *vu* but less than 0.2 *vu* at one site; 3) Unlikely – BVS to IFV more than 0.2 *vu* at one or more sites.

Number	***X*** **site**	***Y*** **site**	***T*** **site**	***W*** **site**	**Bond valence**	**Reason (BVS)**
0.1	N a	AlLiMn^{2+}	Si_6	OH	likely	
0.2	N a	AlLiFe^{2+}	Si_6	OH	likely	
0.3	N a	AlLiMn^{2+}	Si_6	F	likely	
0.4	N a	AlLiFe^{2+}	Si_6	F	likely	
1.1	N a	Al_2Li	Si_5B	OH	likely	
1.2	N a	Al_2Li	Si_5Al	OH	likely	
1.3	N a	Al_3	Si_4B_2	O	likely	
1.3a	N a	Al_3	Si_4B_2	OH	unlikely	high O2
1.3b	N a	Al_3	Si_4B_2	F	unlikely	high O2
1.4	N a	Al_2Li	Si_5B	F	likely	
1.5	N a	Al_2Li	Si_5Al	F	likely	
1.6	N a	Al_2□	Si_6	OH	reasonable	low O2
1.7	N a	Li_2Al	Si_6	F	unlikely	low O2, high *Y*1
1.8	N a	Li_2Al	Si_6	OH	unlikely	low O2, high *Y*1
1.9	N a	Li_3	Si_6	OH	unlikely BVS	low O1 and O2
1.10	N a	Li_3	Si_6	F	unlikely BVS	low O1 and O2
2.1	□	Al_2Li	Si_6	OH	likely	
2.2	□	Al_3	Si_5B	O	likely	
2.3	□	Al_3	Si_5Al	O	likely	
2.4	□	Al_2Li	Si_6	F	likely	
3.	C	Li_2	Si	F	likely	

https://doi.org/10.1180/mgm.2025.28 Published online by Cambridge University Press

1		a		Al		$_{6}$					
	3.		C		Li_2		Si		O	reasonab	high *Y*1
2		a		Al		$_{6}$		H	le		
	3.		C		Al_2		Si		O	likely	
3		a		□		$_{5}$Al		H			
	3.		C		Al_2		Si		O	likely	
4		a		□		$_{5}$B		H			

https://doi.org/10.1180/mgm.2025.28 Published online by Cambridge University Press